Available online at www.sciencedirect.com
ScienceDirect
Proceedings of the Combustion Institute 32 (2009) 99–106
Proceedings of the Combustion Institute
www.elsevier.com/locate/proci

Ab initio chemical kinetics for the reactions of HNCN with $O(^3P)$ and O_2

Shucheng Xu [a], M.C. Lin [a,b,*]

[a] *Department of Chemistry, Emory University, Atlanta, GA 30322, USA*
[b] *Institute of Molecular Science, Department of Applied Chemistry, National Chiao Tung University, Hsichu 300, Taiwan*

Abstract

The kinetics and mechanisms of the reactions of cyanomidyl radical (HNCN) with oxygen atoms and molecules have been investigated by *ab initio* calculations with rate constant prediction. The doublet and quartet state potential energy surfaces (PESs) of the two reactions have been calculated by single-point calculations at the CCSD(T)/6-311+G(*3df*, *2p*) level based on geometries optimized at the CCSD/6-311++G(*d*, *p*) level. The rate constants for various product channels of the two reactions in the temperature range of 300–3000 K are predicted by variational transition state and RRKM theories. The predicted total rate constants of the $O(^3P) + HNCN$ reaction at 760 Torr Ar pressure can be represented by the expressions k_{total} $(O + HNCN) = 3.12 \times 10^{-10} \times T^{-0.05}$ exp $(-37/T)$ $cm^3\,molecule^{-1}\,s^{-1}$ at $T = 300$–3000 K. The branching ratios of primary channels of the $O(^3P) + HNCN$ are predicted: k_1 for producing the NO + CNH accounts for 0.72–0.64, $k_2 + k_9$ for producing the $^3NH + NCO$ accounts for 0.27–0.32, and k_6 for producing the CN + HNO accounts for 0.01–0.07 in the temperature range studied. Meanwhile, the predicted total rate constants of the $O_2 + HNCN$ reaction at 760 Torr Ar pressure can be represented by the expression, $k_{total}(O_2 + HNCN) = 2.10 \times 10^{-16} \times T^{1.28}$exp $(-12200/T)$ $cm^3\,molecule^{-1}\,s^{-1}$ at $T = 300$–3000 K. The predicted branching ratio for $k_{11} + k_{13}$ producing $HO_2 + {}^3NCN$ as the primary products accounts for 0.98–1.00 in the temperature range studied.

Keywords: Chemical kinetics; HNCN reactions with $O(^3P)$ and O_2; Computational study

1. Introduction

The cyanomidyl radical (HNCN) is a reactive transient species which plays an important role in a variety of chemical environments such as in flame, interstellar space, and planetary atmosphere. Experimentally, the HNCN radical was first identified spectroscopically by Herzberg and Warsop in 1963 [1]. More recently, Wu et al. [2] probed the $B^2A' \leftarrow X^2A''$ transition with laser-induced fluorescence, Yamamoto and Saito [3] reported the microwave spectrum of HNCN and Clifford et al. [4] studied the photoelectron spectrum of the $HNCN^-$ ion. In 2001, the photodissociation spectroscopy and dynamics of the HNCN radical have been investigated by Neumark and coworkers [5]. Theoretically, *ab initio* calculations of the molecular geometry and vibrational frequencies of the HNCN ground state were first made by Tao et al. in 1994 [6] and more recently by Puzzarini et al. in 2005 [7]. In our laboratory,

* Corresponding author. Address: Department of Chemistry, Emory University, Atlanta, GA 30322, USA. Fax: +1 404 727 6586.
E-mail addresses: sxu@emory.edu (S. Xu), chemmcl@emory.edu (M.C. Lin).

1540-7489/$ - see front matter © 2009 The Combustion Institute. Published by Elsevier Inc. All rights reserved.
doi:10.1016/j.proci.2008.07.011

we first proposed HNCN to be the key stable intermediate of the prompt NO formation from CH + N_2 along its spin-allowed doublet electronic state path [8].

Under high-pressure conditions, the oxidation of HNCN by OH radical, O(^{3}P) atom, and O_2 molecule may play an important role in the prompt NO formation because they may produce the primary precursors for NO formation, CN, NCN, or NO products, where NCN as one of primary precursors was confirmed in the prompt NO formation experiments recently reported by Smith [9], Hanson and co-workers [10], and Williams and Fleming [11]. Recently, we have studied the kinetics and mechanism of the reaction of HNCN with OH by *ab initio* calculations [12]. In the OH + HNCN study, both singlet and triplet state PESs have been calculated at the CCSD(T)/6-311+G(*3df*, *2p*)//B3LYP/6-311+G(*3df*, *2p*) and CCSD/6-311++G(*d*, *p*) levels of theory and the rate constants for the primary channels of the reaction in the temperature range of 300–3000 K have been predicted. The results show that the primary products are H_2O + NCN at temperatures above 800 K. In present work, we continue to study the chemical kinetics of the reactions of HNCN with O(^{3}P) and O_2 using the similar methods as those employed for the OH + HNCN reaction; there have been no reports on the kinetics and mechanisms for the two reactions experimentally or theoretically.

2. Computational methods

The geometries of the reactants, transition states, intermediate complexes, and products for the O(^{3}P) + HNCN and O_2 + HNCN reactions have been optimized at the CCSD/6-311++G(*d*, *p*) level. The energies for the doublet and quartet state PESs are improved by single point calculations at the CCSD(T)/6-311+G(*3df*, *2p*) level of theory based on the optimized geometries at CCSD/6-311++G(*d*, *p*) level, which have been performed successfully for the reactions of OH + CH_2O [13] and OH + HNCN [12].

The rate constants for the key product channels have been computed with the variational TST and RRKM theory using the Variflex code [14]. All quantum chemistry calculations have been carried out by the Gaussian 03 [15] using a PC cluster and the computers at Cherry L. Emerson Center for Scientific Computation at Emory University.

3. Results and discussion

3.1. Potential energy surfaces and reaction mechanism of the O(^{3}P) + HNCN

The reaction of O(^{3}P) with HNCN can occur on both doublet and quartet reaction channels. The optimized geometries and PESs for the doublet and quartet state reactions are shown in Figs. 1 and 2(a) and (b), respectively.

For the doublet state PES shown in Fig. 2(a), the reaction for O(^{3}P) with HNCN forms firstly primary intermediates D-O-IM_1 (HNCNO) with the binding energy of 53.4 kcal/mol when the O(^{3}P) atom associates with the terminal N atom or D-O-IM_2 (HN(O)CN) with the binding energy of 67.3 kcal/mol when the O(^{3}P) associates with the N atom next to the H atom. D-O-IM_1 and D-O-IM_2 can isomerize to other four intermediates. For example, D-O-IM_1 can transform to D-O-IM_3 (*trans*-HNC(O)N) via D-O-TS_3 with a barrier of 12.5 kcal/mol or to D-O-IM_4 (*cis*-HNC(O)N) via D-O-TS_7 with a barrier of 15.5 kcal/mol. Similarly, D-O-IM_2 can undergo H-atom migration to D-O-IM_6 (HONCN) via D-O-TS_6 with a barrier of 49.1 kcal/mol or O-atom migration to D-O-IM_4 via D-O-TS_8 with a barrier of 44.5 kcal/mol. Furthermore, D-O-IM_3 can isomerize to D-O-IM_5 (HOC(N)N) via D-O-TS_4 with a barrier of 55.3 kcal/mol. There is no direct isomerization pathway found between D-O-IM_1 and D-O-IM_2. However, D-O-IM_1 can transform to D-O-IM_2 through D-O-IM_4. These isomerization reactions can also occur reversely as one would expect. As shown in Fig. 2(a), the doublet state PES of the O(^{3}P) + HNCN reaction may generate the following primary products with the predicted enthalpy changes: NO + CNH, −66.9 kcal/mol; ^{3}NH + NCO, −20.9 kcal/mol; OH + ^{3}NCN, −18.8 kcal/mol; CN + HNO, −2.5 kcal/mol; and ^{3}NH + CNO, 41.7 kcal/mol. The predicted heats of reaction for the formation of

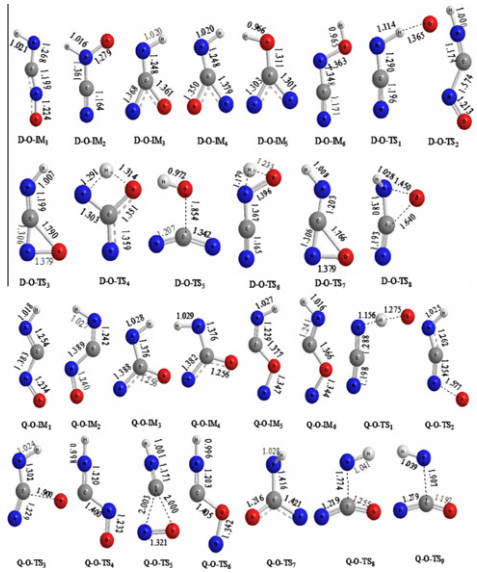

Fig. 1. Optimized geometries of the O(^{3}P) + HNCN reaction computed at the CCSD/6-311++G(*d*, *p*) level.

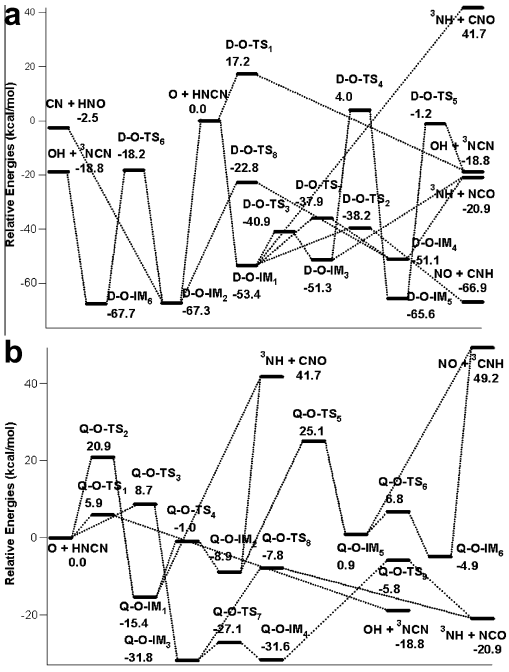

Fig. 2. (a and b) The doublet and quartet state PESs of the O(^{3}P) + HNCN reaction calculated at the CCSD(T)/6-311+G(*3df, 2p*)//CCSD/6-311++G(*d, p*) level.

NO + CNH, OH + ^{3}NCN, and CN+HNO from the O(^{3}P) + HNCN are in reasonable agreement with the available experimental values at 0 K, -66.1 ± 1.6 kcal/mol, -15.4 ± 4.6 kcal/mol, and -2.4 ± 1.4 kcal/mol, respectively, based on the heats of formation $\Delta_f H_0$ at 0 K as the following: $\Delta_f H_0(O) = 59.56 \pm 0.02$ kcal/mol [16]; $\Delta_f H_0(HNCN) = 72.3 \pm 0.7$ kcal/mol [5]; $\Delta_f H_0(NO) = 21.456$ kcal/mol [17]; $\Delta_f H_0(CNH) = 44.3 \pm 0.9$ kcal/mol [5]; $\Delta_f H_0(OH) = 8.87 \pm 0.07$ kcal/mol [16]; $\Delta_f H_0(^3NCN) = 107.6 \pm 3.2$ kcal/mol derived from $\Delta_f H_{298}(^3NCN) = 107.7 \pm 3.2$ kcal/mol [4]; $\Delta_f H_0(CN) = 104.1 \pm 0.5$ kcal/mol [5]; $\Delta_f H_0(HNO) = 24.5$ kcal/mol [17]. Comparing with the available experimental heat of reaction producing ^{3}NH + NCO, -15.2 ± 1.6 kcal/mol based on the experimental heats of formation, $\Delta_f H_0(^3NH) = 85.29 \pm 0.14$ kcal/mol [18] and $\Delta_f H_0(NCO) = 31.36 \pm 0.69$ kcal/mol [19], our predicted value (−20.9 kcal/mol) is about 5.7 ± 1.6 kcal/mol lower than the experimental data. However, the predicted result is close to the value, -21.8 ± 0.7 kcal/mol, based on the computed heats of formation, $\Delta_f H_0(^3NH) = 79.6$ kcal/mol [20] and $\Delta_f H_0(NCO) = 30.5$ kcal/mol [21]. The NO + CNH products are formed by the primary dissociation of the D-O-IM$_1$ by overcoming a small barrier of 15.2 kcal/mol at D-O-TS$_2$. The ^{3}NH + NCO products are from the next key channel by the dissociation of D-O-IM$_3$ and D-O-IM$_4$ with the dissociation energies of 30.4 and 30.2 kcal/mol, respectively. The OH + ^{3}NCN products may be derived from the metathetical process by overcoming a barrier of 17.2 kcal/mol at D-O-TS$_1$, or by the dissociation of the D-O-IM$_5$ through D-O-TS$_5$ with a barrier of 64.4 kcal/mol or D-O-IM$_6$ with a direct dissociation energy of 48.9 kcal/mol. Furthermore, the CN + HNO products may be formed by the direct dissociation of D-O-IM$_2$ with a dissociation energy of 64.8 kcal/mol. Finally, ^{3}NH + CNO may be produced by the direct dissociation of D-O-IM$_1$ with a much higher dissociation energy and thus can be neglected.

For the quartet state PES shown in Fig. 2(b), there is also a direct abstraction channel to produce the OH + ^{3}NCN by overcoming a relatively lower barrier of 5.9 kcal/mol at Q-O-TS$_1$. However, there are no barrierless association processes to form quartet intermediates. The quartet intermediates Q-O-IM$_1$ and Q-O-IM$_3$ are formed from the reactants by overcoming barriers of 20.9 kcal/mol at Q-O-TS$_2$ and 8.7 kcal/mol at Q-O-TS$_3$, respectively. Similar to the doublet state PES, Q-O-IM$_1$, and Q-O-IM$_3$ can isomerize to other intermediates. For example, Q-O-IM$_1$ can isomerize to intermediate Q-O-IM$_2$ via Q-O-TS$_4$ with a barrier of 14.4 kcal/mol, Q-O-IM$_2$ to Q-O-IM$_5$ via Q-O-TS$_5$ with a barrier of 34.0 kcal/mo and Q-O-IM$_5$ to Q-O-IM$_6$ via Q-O-TS$_6$ with a barrier of 5.9 kcal/mol. Meanwhile, Q-O-IM$_3$ can also transform to Q-O-IM$_4$ via Q-O-TS$_7$ with a rotation barrier of 4.7 kcal/mol. These isomerization reactions can also occur reversely as one would expect. As shown in Fig. 2(b), the quartet state PES of the O(^{3}P) + HNCN reaction may generate the following products: OH + ^{3}NCN, ^{3}NH + NCO, ^{3}NH + CNO, and NO + ^{3}CNH. The abstraction channel giving OH + ^{3}NCN is a primary channel. The ^{3}NH + NCO products may be produced by the dissociation of Q-O-IM$_3$ by overcoming a barrier of 24.0 kcal/mol at Q-O-TS$_8$ and Q-O-IM$_4$ by overcoming a barrier of 25.8 kcal/mol at Q-O-TS$_9$, respectively. Furthermore, the products ^{3}NH + CNO and NO + ^{3}CNH formed by direct dissociations with much higher dissociation energies should be negligible.

3.2. Potential energy surfaces and reaction mechanism of the O_2 + HNCN

Analogous to the O(^{3}P) + HNCN reaction, the reaction of O_2 with HNCN can also occur on both doublet and quartet state PESs. The optimized geometries and PESs for the doublet and quartet reaction channels are shown in Figs. 3 and 4(a) and (b), respectively.

For the doublet state PES shown in Fig. 4(a), the reactants O_2 + HNCN have to overcome 34–40 kcal/mol barriers to form doublet intermediates except for forming D-O$_2$-IM$_1$ by overcoming 12.0 kcal/mol at D-O$_2$-TS$_1$ because of its loose

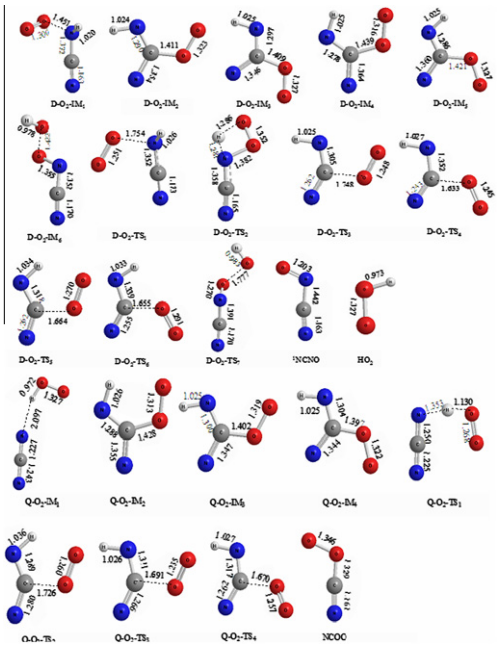

Fig. 3. Optimized geometries of the $O_2 + HNCN$ reaction computed at the CCSD/6-311++G(*d*, *p*) level.

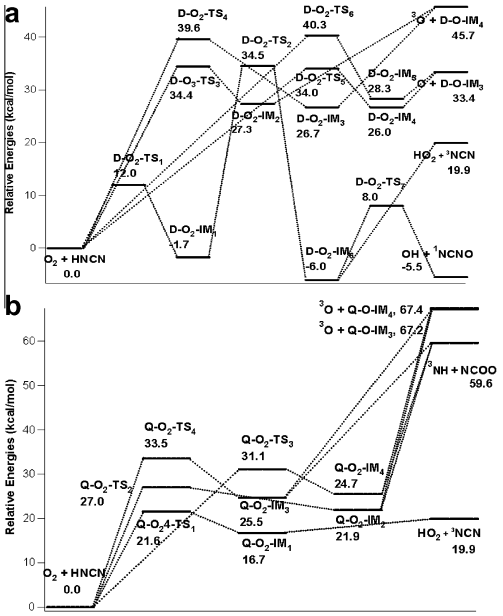

Fig. 4. (a and b) The doublet and quartet state PESs of the $O_2 + HNCN$ reaction calculated at the CCSD(T)/6-311+G(*3df, 2p*)//CCSD/6-311++G(*d*, *p*) level.

structure for O_2-N(H)CN. In addition, the direct O-abstraction channel for O_2 attacking NCNH producing O + HNCNO in the doublet state is neglected due to its 78 kcal/mol barrier. The D-O_2-IM_6 may dissociate to products OH + ^{1}NCNO by overcoming a barrier of 14.0 kcal/mol at D-O_2-TS_7 or HO_2 + ^{3}NCN with the dissociation energy of 25.9 kcal/mol. In addition, the D-O_2-IM_4 and D-O_2-IM_5 may dissociate directly to products O + D-O-IM_3 with the dissociation energies of 7.4 and 5.2 kcal/mol, respectively. Finally, the D-O_2-IM_2 and D-O_2-IM_3 may dissociate directly to products O + D-O-IM_4 with the dissociation energies of 18.4 and 19.0 kcal/mol, respectively.

The quartet state PES shown in Fig. 4(b) is similar to the doublet state PES. However, the reactants O_2 + HNCN have to overcome relatively lower barriers of 22-34 kcal/mol to form quartet intermediates Q-O_2-IM_1, Q-O_2-IM_2, Q-O_2-IM_3, and Q-O_2-IM_4. The Q-O_2-IM_1 is a product complex, which can dissociate directly to products HO_2 + ^{3}NCN with a lower dissociation energy of 3.2 kcal/mol. Similarly as in the doublet state, the direct O-abstraction channel for O_2 attacking NCNH to produce O + HNCNO in the quartet state is neglected due to its high (83 kcal/mol) barrier. Finally, the direct dissociation processes can also occur from Q-O_2-IM_2, Q-O_2-IM_3, and Q-O_2-IM_4 to produce ^{3}NH + NCOO, O + Q-O-IM_3, and Q-O-IM_4 with considerably higher dissociation energies, they should be negligible.

3.3. Rate constants calculations for the primary reaction channels of the $O(^3P)$ + HNCN and O_2 + HNCN

3.3.1. Methods employed for rate constant calculations

The rate constants for the following primary doublet and quartet state reaction channels of the $O(^3P)$ + HNCN and O_2 + HNCN have been predicted using variational TST and RRKM theory by the Variflex Code[14] in the temperature range 300–3000 K and pressure range of 1–7600 Torr based on the obtained PESs at the CCSD(T)/6-311+G(*3df*, *2p*) level with the optimized structures at the CCSD/6-311++G(*d*, *p*) level:

$$O + HNCN \rightarrow D\text{-}O\text{-}IM_1^* \rightarrow NO + CNH \quad (1)$$
$$\rightarrow {}^3NH + NCO \quad (2)$$
$$\rightarrow OH + {}^3NCN \quad (3)$$
$$O + HNCN \rightarrow D\text{-}O\text{-}IM_2^* \rightarrow D\text{-}O\text{-}IM_2(+M) \quad (4)$$
$$\rightarrow OH + {}^3NCN \quad (5)$$
$$\rightarrow CN + HNO \quad (6)$$
$$O + HNCN \rightarrow D\text{-}O\text{-}TS_1 \rightarrow OH + {}^3NCN \quad (7)$$
$$O + HNCN \rightarrow Q\text{-}O\text{-}TS_1 \rightarrow OH + {}^3NCN \quad (8)$$
$$O + HNCN \rightarrow Q\text{-}O\text{-}TS_3 \rightarrow {}^3NH + NCO \quad (9)$$
$$O_2 + HNCN \rightarrow D\text{-}O_2\text{-}TS_1 \rightarrow OH + NCNO \quad (10)$$
$$\rightarrow OOH + {}^3NCN \quad (11)$$

$$O_2 + HNCN \rightarrow D\text{-}O_2\text{-}TS_4 \rightarrow O + D\text{-}O\text{-}IM_3 \quad (12)$$

$$O_2 + HNCN \rightarrow Q\text{-}O_2\text{-}TS_1 \rightarrow OOH + {}^3NCN \quad (13)$$

where Channels (1)–(7) are the doublet channels and Channels (8), (9) are the quartet channels of the $O(^3P) + HNCN$ reaction and Channels (10)–(12) are the doublet channels and Channel (13) is the quartet channel of the $O_2 + HNCN$ reaction. Here the formation of D-O-IM_1 is negligible because the dissociation barriers for production of NO + CNH and ^3NH + NCO are small and thus no significant stabilization of intermediate is expected.

Channels (1)–(5), (6), (12), (13) involve barrierless association processes or direct dissociation processes, which are treated using the variational TST. The minimum energy paths (MEPs) for O + HNCN → D-O-IM_1 (MEP_1), O + HNCN → D-O-IM_2(MEP_2), D-O-IM_2 → CN + HNO (MEP_3), D-O-IM_3 → ^3NH + NCO (MEP_4), D-O-IM_4 → ^3NH + NCO (MEP_5), D-O-IM_6→ OH + ^3NCN (MEP_6), D-O_2-IM_6 → HO_2 + ^3NCN (MEP_7), D-O_2-IM_4 → O + D-O-IM_3(MEP_8), and Q-O_2-IM_1→ HO_2 + ^3NCN (MEP_9), were obtained by computing the potential energy curves along the reaction coordinate from their equilibrium bond length to 5.0 Å with a step size of 0.1 Å estimated at the UB3LYP/6-311+G(*3df*, *2p*) level. The calculated MEPs for the above-mentioned processes could be fitted to the Morse potential function with the parameters, $\beta = 2.600$ Å^{-1} with $R_0 = 1.220$ Å, and $D_e =$ 56.4kcal/mol for MEP_1; $\beta = 2.960$ Å^{-1} with $R_0 =$ 1.2767 Å, and $D_e = 71.5$ kcal/mol for MEP_2; $\beta = 2.220$ Å^{-1} with $R_0 = 1.346$ Å, and $D_e = 69.3$ kcal/mol for MEP_3; $\beta = 2.485$ Å^{-1} with $R_0 =$ 1.238 Å, and $D_e = 35.8$ kcal/mol for MEP_4; $\beta = 4.471$ Å^{-1} with $R_0 = 1.238$ Å, and $D_e = 35.7$ kcal/mol for MEP_5; $\beta = 2.984$ Å^{-1} with $R_0 =$ 1.367 Å, and $D_e = 54.9$ kcal/mol for MEP_6; $\beta = 4.718$ Å^{-1} with $R_0 = 1.356$ Å, and $D_e =$ 29.9 kcal/mol for MEP_7; $\beta = 4.012$ Å^{-1} with $R_0 =$ 1.318 Å, and $D_e = 8.6$ kcal/mol for MEP_8; $\beta = 1.615$ Å^{-1} with $R_0 = 1.990$ Å, and $D_e = 4.3$ kcal/mol for MEP_9; respectively, where the energies for D_e were scaled to the CCSD(T)//CCSD level without ZPE corrections. For the variational rate constant calculations by the Variflex code, a statistical treatment of the transitional-mode contributions to the transition-state partition functions was performed variationally. The numbers of states are evaluated according to the variable reaction coordinate flexible transition state theory [14,22]. The energy-transfer process was computed on the basis of the exponential down model with the $\langle \Delta E \rangle_{down}$ value of 400 cm^{-1} for Ar. The Morse potentials with the above-mentioned parameters, the Lennard-Jones pair-wise potential and the anisotropic potential are added together to form the final potential, similar to that employed in the OH + CH_2O [13], OH + CH_3OH [23], OH + C_2H_5OH [23], and OH + HNCN [12] reactions. For the Lennard-Jones potential, the function of $V_{LJ} = 4\varepsilon\ [(\sigma/r)^{12} - (\sigma/r)^6]$ was used, where r is the distance between the non-bonding atoms, ε is the well depth and σ is the hard sphere radius. In this calculation, ε and σ are 42.80 cm^{-1}, 2.95 Å; 35.6 cm^{-1}, 3.35 Å; 25.90 cm^{-1}, 3.31 Å; and 5.98 cm^{-1}, 2.81 Å for O, C, N, and H atoms, respectively, as recommended in the Variflex code [14]. For the anisotropic potential, the stretching potential is used in conjunction with the potential form of $V_{Ani} = V_0[1 - (\cos^2(\theta_1 - \theta_{1e}) \times \cos^2(\theta_2 - \theta_{2e})]$. Where, V_0 is the stretching potential which is represented by a Morse potential in this work as mentioned above; θ_1 and θ_2 are the rotational angles between the fragments 1 and 2 and the reference axis; θ_{1e} and θ_{2e} represent the equilibrium bonging angles of fragments 1 and 2.

The tunneling effect on the transition states, D-O-TS_1 in Channel (7), Q-O-TS_1 in Channel (8), Q-O-TS_3 in Channel (9), D-O_2-TS_1 in Channel (10), D-O_2-TS_4 in Channel (12), and Q-O_2-TS_1 in Channel (13) are considered because their barriers are higher than the reactants [13,23]. In this study, the tunneling effects are treated using the Eckart's tunneling corrections.

3.3.2. Predicted rate constants for $O(^3P)$ + HNCN

For the reaction channels of the $O(^3P)$ + HNCN, only k_4 forming D-O-IM_2 has a strong pressure dependence in the temperature range of 300–3000 K. When the pressure increases from 1 Torr to 10 atmospheres, k_4 producing HN(O)CN (shown in Figure S1 of Supplemental data) increases too. In addition, the values of k_4 decrease with increasing temperature from 300 to 3000 K. The rate constants k_1, k_2, k_3, k_5, k_6, k_7, k_8, and k_9 have no pressure dependence in the whole temperature range. The predicted individual and total rate constants for the primary products at 760 Torr Ar pressure in the temperature range of 300–3000 K are shown in Fig. 5(a). As shown in the figure, the primary products of the $O(^3P)$ + HNCN reaction are NO + CNH with the rate constants (1.26–1.53) × 10^{-10} cm^3 molecule^{-1} s^{-1} in the whole temperature range investigated. The second, third, and fourth key products are the ^3NH + NCO with the rate constants in the range (5.70–6.70) × 10^{-11} cm^3 molecule^{-1} s^{-1}, the CN + HNO with the rate constants in the range (2.59–14.30) × 10^{-12} cm^3 molecule^{-1} s^{-1}, and the OH + ^3NCN with the rate constants varying in the range (2.30–6.74) × 10^{-13} cm^3 molecule^{-1} s^{-1}, respectively. The production of D-O-IM_2 through collisional quenching is negligible.

The total rate constant k_{total} (O + HNCN)= $\sum k_i$ for all accessible channels have no pressure dependence either in the temperature range 300–3000 K because the primary channels have no pressure effects.

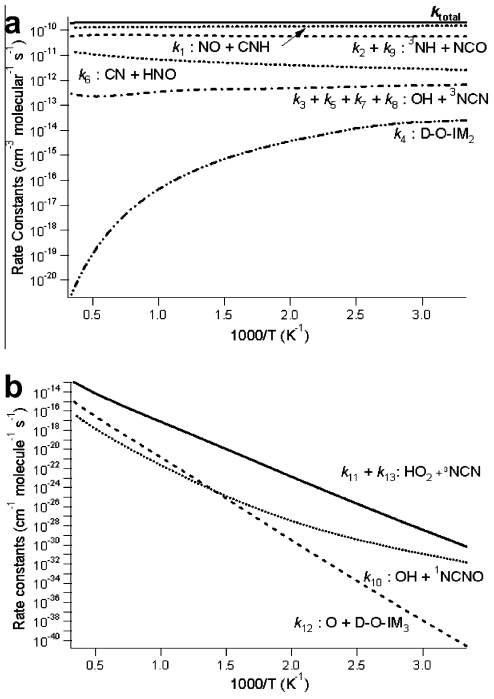

Fig. 5. (a) The predicted rate constants of individual products and k_{total} of the O(^{3}P) + HNCN reaction at the 760 Torr Ar pressure in the temperature range of 300–3000 K. (b) The predicted rate constants of individual products of the O_2 + HNCN reaction at the 760 Torr Ar pressure in the temperature range of 300–3000 K.

The predicted individual and total rate constants given in units of cm^3 molecule^{-1} s^{-1} at the 760 Torr Ar pressure in the temperature range 300–3000 K can be represented by:

$$k_1 = 2.46 \times 10^{-10} \times T^{-0.08} \exp(-11/T),$$
$$k_2 = 1.90 \times 10^{-10} \times T^{-0.13} \exp(-156/T),$$
$$k_3 = 6.64 \times 10^{-28} \times T^{4.02} \exp(-1288/T),$$
$$k_4 = 1.57 \times 10^{+16} \times T^{-10.47} \exp(-2675/T),$$
$$k_5 = 3.46 \times 10^{-15} \times T^{0.47} \exp(844/T),$$
$$k_6 = 1.05 \times 10^{-13} \times T^{0.62} \exp(-95/T),$$
$$k_7 = 5.89 \times 10^{+4} \times T^{-5.79} \exp(-8674/T),$$
$$k_8 = 2.45 \times 10^{-2} \times T^{-3.37} \exp(-2732/T),$$
$$k_9 = 1.43 \times 10^{+2} \times T^{-5.14} \exp(-5039/T),$$
$$k_{total}(O + HNCN) = 3.12 \times 10^{-10} \times T^{-0.05} \exp(-37/T).$$

Comparing with the OH + HNCN reaction [12], k_{total} (O + HNCN) is 2–15 times larger than that of the OH + HNCN at $T > 500$ K under the atmospheric pressure condition. In addition, the primary products of O(^{3}P) + HNCN are NO + CNH instead of H_2O + NCN in the OH + HNCN reaction. Therefore, the O + HNCN reaction may be as important as OH + HNCN for prompt NO production.

3.3.3. Predicted rate constants for O_2 + HNCN

In the O_2 + HNCN reaction, all product channels have no pressure dependence in the whole temperature range studied. The predicted individual rate constants for the primary products at 760 Torr Ar pressure in the temperature range of 300–3000 K are shown in Fig. 5(b). As shown in Fig. 5(b), the primary products for the O_2 + HNCN are the HO_2 + ^{3}NCN with the rate constants ranging from 6.62×10^{-31} to 1.09×10^{-13} cm^3 molecule^{-1} s^{-1} in the whole temperature range. The other products OH + NCNO with the rate constants varying in the range 1.53×10^{-32}–4.87×10^{-17} cm^3 molecule^{-1} s^{-1} and O + D-O-IM$_3$ in the range 2.62×10^{-41}–1.00×10^{-15} cm^3 molecule^{-1} s^{-1} are small and can be neglected.

The predicted individual and total rate constants given in units of cm^3 molecule^{-1} s^{-1} at the 760 Torr Ar pressure in the temperature range 300–3000 K can be represented by:

$$k_{10} = 1.38 \times 10^{-45} \times T^{8.55} \exp(-6090/T),$$
$$k_{11} = 1.72 \times 10^{-34} \times T^{5.92} \exp(-10900/T),$$
$$k_{12} = 3.29 \times 10^{-15} \times T^{0.64} \exp(-19200/T),$$
$$k_{13} = 2.67 \times 10^{-16} \times T^{1.25} \exp(-12300/T),$$
$$k_{total}(O_2 + HNCN) = 2.10 \times 10^{-16} \times T^{1.28} \exp(-12200/T).$$

Comparing with the OH + HNCN and O(^{3}P) + HNCN reactions, $k_{total}(O_2 + HNCN)$ with the rate constants of 6.77×10^{-31}–1.10×10^{-13} cm^3 molecule^{-1} s^{-1} in the whole temperature range are much smaller than those of the OH + HNCN [12] and O(^{3}P) + HNCN reactions. The results are similar to those predicted for the NCN reactions with O, OH, and O_2, in which the molecular oxygen reaction was found to be extremely slow due to its high reaction barrier [24,25].

3.3.4. Predicted branching ratios

The branching ratios of the products for the O(^{3}P) + HNCN and O_2 + HNCN at the 760 Torr Ar-pressure in the temperature range of 300–3000 K are shown in Fig. 6(a) and (b), respectively. For the O(^{3}P) + HNCN reaction, k_1 for producing the NO + CNH accounts for 0.72–0.64, $k_2 + k_9$ for producing the ^{3}NH + NCO accounts for 0.27–0.32, and k_6 for producing the CN + HNO accounts for 0.01–0.07 in the temperature range of 300–800 K. The branching ratios of $k_3 + k_5 + k_7 + k_8$ for producing the OH + ^{3}NCN and k_4 for forming D-O-IM$_2$ are negligible in the whole temperature range. For the

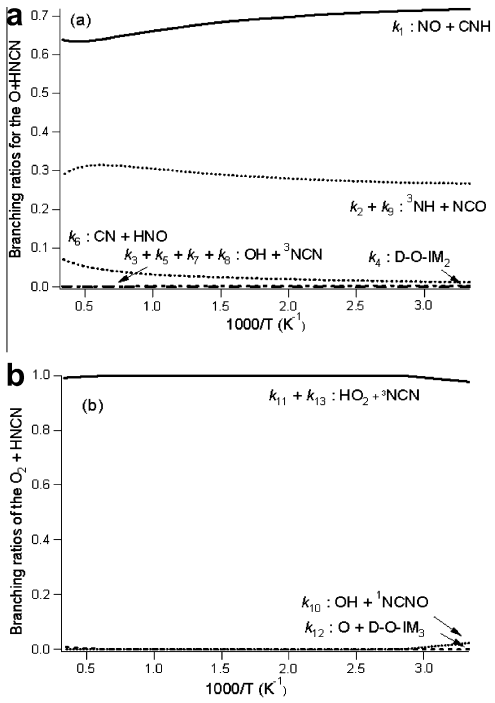

Fig. 6. (a and b) The predicted branching ratios for the products of the O(^{3}P) + HNCN and O_2 + HNCN reactions at the 760 Torr Ar pressure in the temperature range 300–3000 K.

O_2 + HNCN reaction, $k_{11} + k_{13}$ for producing the $HO_2 + {}^3$NCN accounts for 0.98–1.00. The branching ratios of k_{10} for producing the OH + ^{1}NCNO and k_{12} for producing the O + D-O-IM_3 are negligible in the whole temperature range studied.

4. Conclusions

The kinetics and mechanisms for the O(^{3}P) + HNCN and O_2 + HNCN reactions taking place via the doublet and quartet state PESs have been studied at the CCSD(T)/6-311+G(*3df*, *2p*)//CCSD/6-311++G(*d*, *p*) level of theory. The total and individual rate constants for the primary channels of the two reactions in the temperature range of 300–3000 K are predicted. The total rate constants of the O(^{3}P) + HNCN reaction producing the primary products of NO + CNH is 2–15 times larger than that of the OH + HNCN producing the primary products of H_2O + NCN when the temperature is over 500 K. However, the total rate constants of the O_2 + HNCN reaction producing the primary products, $HO_2 + {}^3$NCN, are much slower than those for the OH + HNCN or O + HNCN reactions due to the much higher reaction barriers. Our predicted total and individual rate constants, and product branching ratios for the O(^{3}P) + HNCN and O_2 + HNCN reactions may be employed for combustion kinetic modeling of prompt NO formation.

Acknowledgements

The authors are grateful for the support of this work from the Basic Energy Sciences, Department of Energy, under contract no. DE-FG02-97-ER14784. MCL acknowledges the support by Taiwan's National Science Council for a distinguished visiting professorship at National Chiao Tung University, Hsinchu, Taiwan.

Appendix A. Supplementary data

Supplementary data associated with this article can be found, in the online version, at doi:10.1016/j.proci.2008.07.011.

References

[1] G. Herzberg, D.N. Travis, *Can. J. Phys.* 41 (1963) 286.
[2] M. Wu, G. Hall, T.J. Sears, *J. Chem. Soc. Faraday Trans.* 89 (1993) 615.
[3] S. Yamamoto, S. Saito, *J. Chem. Phys.* 101 (1994) 10350.
[4] E.P. Clifford, P.G. Wenthold, W.C. Lineberger, G. Petersson, G.B. Ellison, *J. Phys. Chem. A* 101 (1997) 4338.
[5] R.T. Bise, A.A. Hoops, D.M. Neumark, *J. Chem. Phys.* 114 (2001) 9000.
[6] F.-M. Tao, W. Klemperer, P. Thaddeus, *J. Chem. Phys.* 100 (1994) 3691.
[7] C. Puzzarini, A. Gambi, *J. Chem. Phys.* 122 (2005) 064316.
[8] L.V. Moskaleva, W.S. Xia, M.C. Lin, *Chem. Phys. Lett.* 331 (2000) 269–277.
[9] G.P. Smith, *Chem. Phys. Lett.* 367 (2002) 541–548.
[10] V. Vasudevan, R.K. Hanson, C.T. Bowman, D.M. Golden, D.F. Davidson, *J. Phys. Chem. A* 111 (2007) 11818–11830.
[11] B.A. Williams, J.W. Fleming, *Proc. Combust. Inst.* 31 (2007) 1109–1117.
[12] S.C. Xu, M.C. Lin, *J. Phys. Chem. A* 111 (2007) 6730.
[13] S.C. Xu, R.S. Zhu, M.C. Lin, *Int. J. Chem. Kinet.* 28 (2006) 322–326.
[14] S.J. Klippenstein, A.F. Wagner, R.C. Dunbar, D.M. Wardlaw, S.H. Robertson, *Variflex* (1999).
[15] M.J. Frisch, J.A. Pople, et al., *Gaussian 03, Revision A.7*; Gaussian, Inc.: Pittsburgh, PA, 2003.
[16] B. Ruscic, J.E. Boggs, A. Burcat, et al., *J. Phys. Chem. Ref. Data* 34 (2005) 573–656.
[17] M.W. Chase Jr., *NIST-JANAF Thermochemical Tables*, fourth ed., J. Phys. Chem. Ref. Data, Monograph 9, Woodbury, New York (1998) 1–1951.

[18] R. Tarroni, P. Palmieri, A. Mitrushenkov, P. Tosi, D. Bassi, *J. Chem. Phys.* 106 (1997) 10265.
[19] A.A. Hoops, R.T. Bise, J.R. Gascooke, D.M. Neumark, *J. Chem. Phys.* 114 (2001) 9020.
[20] B.S. Jursic, *Theor. Chem. Acc.* 99 (1998) 171–174.
[21] M.S. Schuurman, S.R. Muir, W.D. Allen, H.F. Schaefer III, *J. Chem. Phys.* 120 (2004) 11586–11599.
[22] R.G. Gilbert, S.C. Smith, *Theory Unimol. React. Blackwell* (1990).
[23] S.C. Xu, M.C. Lin, *Proc. Combust. Inst.* 31 (2007) 159–166.
[24] R.S. Zhu, M.C. Lin, *J. Phys. Chem. A* 111 (2007) 6766–6771.
[25] R.S. Zhu, M.C. Lin, *Int. J. Chem. Kinet.* 37 (2005) 593–598.